3J3-3

Implementation of Self-Bending Airborne Ultrasonic Beam with a Reflector for Phase-Coded Modulation

反射板を利用した位相符号化制御による空中超音波ビームベンディングの実装

Nagisa Yamamoto‡, Hideyuki Nomura (Univ. of Electro-Comm.)
山本 凪紗‡，野村 英之 (電通大)

1. Introduction

Acoustic self-bending beam is an appealing phenomenon, which can generate a beam supernaturally along a curving trajectory [1]. Particularly, the beam bending for airborne ultrasound has a large expectation for some applications requiring control of sound fields such as audible area control for parametric loudspeakers [2].

A method for generating a self-bending ultrasonic beam in air is the phase-coded modulation which translates the Airy function into an initial spatial phase distribution in the binary form expressed by 0 and π [3]. The self-bending airborne ultrasonic beam based on the Airy function has been implemented approximately by controlling the amplitude of the sound source in binary, instead of the phase [2]. However, it makes numerous sidelobes aside from bending the main lobe, resulting in a weak convergence of sound pressure into the main lobe. Hence, it is required to invent another way to implement the phase-coded modulation in order to utilize the self-bending airborne ultrasonic beam as a basis for certain applications.

In this study, we propose a new method that adjusts the spatial phase distribution of sound waves with the reflector for implementing a self-bending airborne ultrasonic beam. We designed the reflector based on the phase-coded modulation, fabricated with a universal 3D printer and experimentally evaluated the sound field when with the manufactured reflector.

2. Methodology

2.1. Explanation of phase-coded modulation

A spatial phase pattern for the design of the reflector was determined based on the phase-coded modulation. First, it is assumed that $\Phi(u) = \mathrm{Ai}(bu)e^{au}$, where $\mathrm{Ai}(bu)$ is the Airy function [3]. Here, the spatial phase distribution $\theta(u)$ derived from $\Phi(u)$ is defined as 0 and π, for $\Phi(u) < 0$ and $\Phi(u) > 0$, respectively [3].

2.2. Design of a reflector

The phase was adjusted by using a reflector as described in **Fig. 1**. The difference in the distance that sound waves would reach the virtual radiating surface from the sound source surface through each path P_A and P_B is $d/\cos\alpha$, where α is the incident angle and d is the thickness of the reflector. If the phase difference of the two sound waves on the radiating surface is equal to π, then the difference $d/\cos\alpha$ is equal to $\lambda/2$ where λ is the wavelength.

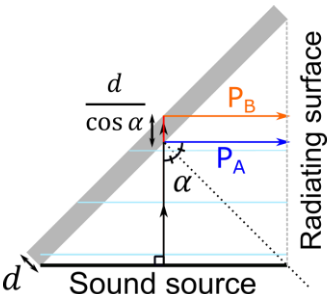

Fig. 1 The diagram for explanation of phase delay.

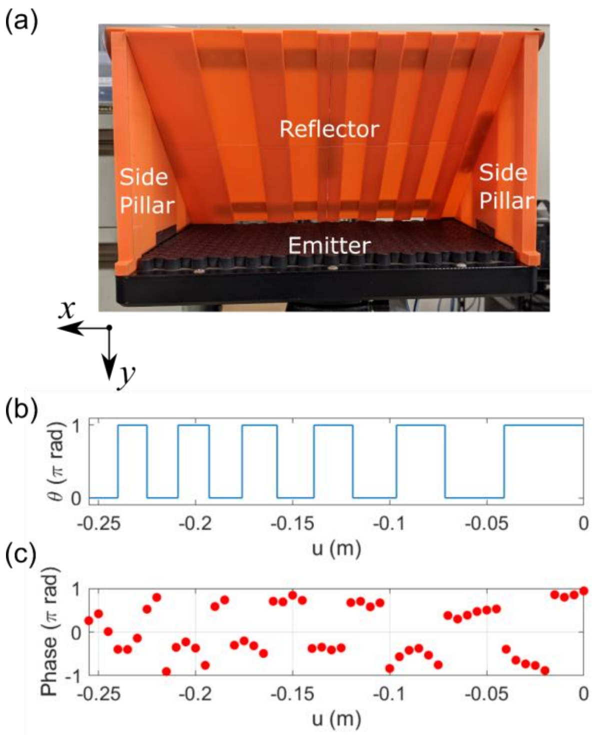

Fig. 2 (a)The fabricated reflector mounting with the emitter. (b) The spatial phase distribution that was designed and (c)measured the manufactured reflector.

A reflector was designed for $d = 3$ mm, $\alpha = 45°$, frequency $f = 40$ kHz and the sound speed $c = 340$ m/s, and verified theoretically and experimentally.

Next, we implemented the phase shifter by setting steps whose height is 3 mm on the reflector

E-mail: nagisa.yamamoto@uec.ac.jp, h.nomura@uec.ac.jp

for the position corresponding to the areas whose $\theta = \pi$ rad in the spatial phase distribution and no steps to the areas of 0 rad. We performed 3D printing to manufacture the reflector depicting the same pattern as $\Phi(u)$, expressing with the steps of 3 mm. We determined the spatial phase distribution based on the phase-coded modulation with parameters $a = 1\ \mathrm{m}^{-1}$, $b = 57\ \mathrm{m}^{-1}$ in $\Phi(u)$, and with the total length of 255 mm to fit the ultrasonic emitter we used for experiments.

The fabricated reflector is shown in **Fig. 2(a)**. In order to keep the incident angle stable, side pillars were mounted on both sides of an ultrasonic emitter.

2.3 Evaluation of the reflector

We examined the spatial phase distribution of the reflector by scanning a microphone along the *x*-axis perpendicular to the radiational direction of the emitter and the range direction *z* on the radiation surface. **Figures 2(b) and (c)** show the initial phase distribution θ designed in Chap. 2.2 and the phase distribution measured in the experiment. This result proves that the manufactured reflector reflects the incoming waves with shifts in their phase as designed.

3. Evaluation of the sound field

3.1 Preparation

We observed the sound field when mounting the reflector on the emitter. The block diagram of the experimental setting is shown in **Fig.3**. The driving frequency of the emitter was 40 kHz. The sound pressure was measured by traversing a microphone in the sound field.

Also, we demonstrated the sound field with FEM in 2D for the configuration that a sound source has the spatial phase distribution described in Fig.2(b) [2]. For simulation, the driving frequency was set same value as the experiment. The pressure amplitude of the sound source was set to 1 Pa. The sound source was located along the *x*-axis, perpendicular to the range direction *z*-axis. Sommerfeld radiation condition was applied as the outer boundary condition [2].

3.2 Results and Discussions

The sound pressure level (SPL) measured on the sound field is plotted in **Fig. 4**. Each figure describes the results for each distance from the emitter. It can be seen that the SPL for when with reflector has a peak at $(x, z) = (12.5\ \mathrm{cm}, 0.4\ \mathrm{m})$ and the peak shifts to the direction of increasing x as the distance getting further, resulting in the peak at $(x, z) = (22.5\ \mathrm{cm}, 1.0\ \mathrm{m})$. Apart from the slight discordance of the peaks' position, this measurement agrees with the result of the simulation. This result shows that the proposed method could generate a self-bending main lobe with 40 kHz-ultrasound in air.

4. Conclusion

A method for implementing a self-bending ultrasonic beam in air, which uses a reflector that was designed based on phase-coded modulation and was easily fabricated, was proposed in this study. It is experimentally proven that the proposed method can generate the self-bending airborne ultrasonic beam.

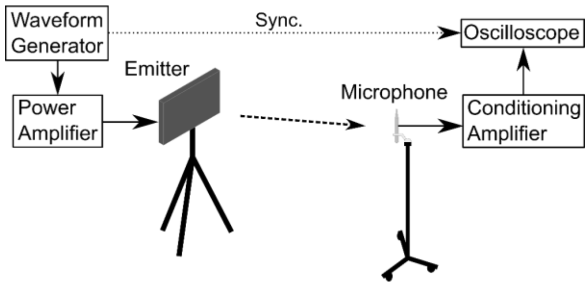

Fig. 3 The diagram of the experimental setup.

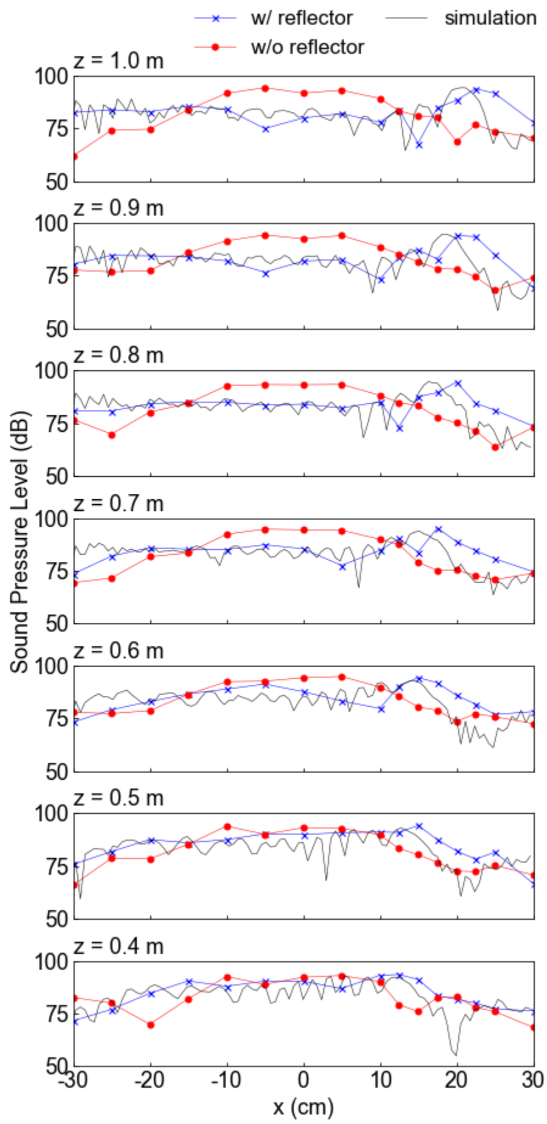

Fig. 4 The sound pressure level of the field.

References

1. P. Zhang, T. Li, J. Zhu, X. Zhu, S. Yang, Y. Wang, X. Yin and X. Zhang: Nat. Commun. **5** (2014) 4316.
2. N. Yamamoto and H. Nomura: Jpn. J. Appl. Phys.,**60** (2021) SDDB05.
3. D.-C. Chen, X.-F. Zhu, D.-J. Wu and X.-J. Liu: Appl. Phys. Lett. **114** (2019) 053504.